COMPARISON OF OXIDE- AND METAL-CORE BEHAVIOR DURING CRBRP STATION BLACKOUT

S. T. Polkinghorne
S. A. Atkinson

Idaho National Engineering Laboratory

EG&G Idaho, Inc.

EGG-M--01086

DE88 001601

Abstract

A resurrected concept that could significantly improve the inherently safe response of Liquid-Metal cooled Reactors (LMRs) during severe undercooling transients is the use of metallic fuel. Analytical studies have been reported on for the transient behavior of metal-fuel cores in innovative, inherently safe LMR designs. This paper reports on an analysis done, instead, for the Clinch River Breeder Reactor Plant (CRBRP) design with the only innovative change being the incorporation of a metal-fuel core. The SSC-L code was used to simulate a protected station blackout accident in the CRBRP with a 943 MWt Integral Fast Reactor (IFR) metal-fuel core. The results, compared with those for the oxide-fueled CRBRP, show that the margin to boiling is greater for the IFR core. However, the cooldown transient is more severe due to the faster thermal response time of metallic fuel. Some additional calculations to assess possible LMR design improvements (reduced primary system pressure losses, extended flow coastdown) are also discussed.

Introduction

The concept of "walk away" safety has prompted renewed interest in the use of metallic fuel in innovative Liquid-Metal cooled Reactor (LMR) designs. Metallic fuel, similar to that used in EBR-II, could significantly improve the inherently safe response of LMRs during severe undercooling transients. This paper presents an analysis of a protected station blackout in a loop-type LMR containing a metal-fuel core. The results are compared with those obtained for a more traditional oxide-fueled LMR. The calculations were performed using the SSC-L code (Super System Code - Loop version) [1]. The metal-core design was based on Argonne National Laboratory's Integral Fast Reactor (IFR) concept [2] and the vessel and heat transport system were adapted from a Brookhaven National Laboratory model of the Clinch River Breeder Reactor Plant (CRBRP). The heterogeneous CRBRP oxide-core served as the basis for comparison.

Model Description

The IFR core was modeled by five fuel/coolant channels. The first represented the hot pin in the peak core assembly and the second represented all 108 fuel assemblies (driver assemblies) of the IFR core. Each IFR fuel assembly contains 271 uranium-plutonium-zirconium fuel pins. Channel three represented the hot pin in the peak blanket assembly and channel four represented all 42 assemblies of the radial blanket. The blanket assemblies each contain 127 depleted uranium fuel pins. The fifth channel represented the 13 primary and secondary control assemblies. Each control assembly was assumed to contain 37 boron carbide control pins (same as the CRBRP). A core bypass channel was also modeled and was assumed to include all radial shield assemblies.

The CRBRP core model included two additional fuel/coolant channels: one representing the hottest internal blanket pin, and the other representing all of the internal blanket assemblies. The CRBRP core contains 162 driver assemblies, 76 internal blanket assemblies, 126 radial blanket assemblies, and 15 control assemblies. Each fuel assembly contains 217 mixed oxide fuel pins, each blanket assembly contains 61 depleted uranium dioxide fuel pins, and each control assembly contains 37 boron carbide control pins. All radial shield assemblies were assumed to be contained in a core bypass channel.

Several IFR metal-core and CRBRP oxide-core design parameters are compared in Table 1. The IFR data are for a preliminary homogeneous core design [3]; the numbers in parentheses are assumed values. The power generated in each IFR core region corresponds to beginning-of-life conditions. To simulate the hottest IFR pin, a conservative factor of 1.15 was applied to the average pin in the peak power assembly. The IFR axial power factors (not shown) were assumed to be the same as for the CRBRP. The homogeneous arrangement of the IFR core is compared to the heterogeneous CRBRP configuration in Figure 1.

The three parallel heat transport circuits of the CRBRP, each consisting of a primary and intermediate sodium loop and a tertiary water/steam loop, were modeled by one equivalent set of loops. The primary loop was modeled by piping, a primary pump, the shell side of the intermediate heat exchanger (IHX), and a check valve. The intermediate loop was modeled by piping, the tube side of the IHX, the shell sides of the superheater and evaporator (the two evaporators were lumped), and an intermediate pump. The steam generating loop consisted of piping, the tube sides of the evaporator and superheater, a recirculation pump, a steam drum, valves, a steam header, and appropriate boundary conditions. The configuration of the CRBRP heat transport system is illustrated in Figure 2.

For the metal-core model, the CRBRP intermediate loop flow rate, main feedwater flow rate, and protected air-cooled condenser (PACC) heat transfer rate were all scaled by the ratio of IFR metal-core thermal power to CRBRP oxide-core thermal power (943/975 MWt). The vessel nozzle-to-nozzle pressure drop was scaled by the square of the ratio of IFR to CRBRP primary system mass flow rate $(4558/5228\ kg/s)^2$.

Code Modifications

To simulate IFR-type metallic fuel, it was necessary to modify some of the material property correlations in SSC-L. The temperature-dependent correlations for thermal conductivity, specific heat capacity, and average coefficient of thermal expansion are currently only valid for oxide fuel. Therefore, some preliminary metallic fuel data [4] were correlated (least squares polynomial fits) and encoded in SSC-L. The gap conductance model was also modified to simulate sodium-bonded fuel pins.

The IFR will be fueled with U-Zr initially followed by U-Pu-Zr reloads. The current reference fuel composition is U-15 wt% Pu-10 wt% Zr. The axial and radial blankets will contain depleted uranium metal. Figure 3 compares the properties of metallic and oxide fuel. The data are shown up to each material's melting point: ~1430 and 3020 K for U-Pu-Zr and UO_2-PuO_2, respectively.

The higher thermal conductivity of metallic fuel results in less stored energy and a faster thermal response time than oxide fuel. The larger thermal expansion coefficient results in a more pronounced negative reactivity feedback effect (due to axial expansion) than oxide fuel. Both characteristics are important considerations

in the design of inherently safe LMRs. The density of fuel material is computed in SSC-L using the thermal expansion data shown in Figure 3 and room temperature densities of 15800 and 11040 kg/m³ for U-15 wt% Pu-10 wt% Zr and UO_2-20 wt% PuO_2, respectively.

Steady State Results

The results from the steady state calculations are compared in Table 2. As shown, the IFR hot pin generates 57% more power than the CRBRP hot pin. However, because of the metallic fuel pin's higher thermal conductivity and gap conductance, the peak fuel temperature is 1162 K less than the oxide pin. Figure 4 shows fuel centerline temperature profiles along the length of the hot IFR and CRBRP fuel pins during steady state operation. The figure illustrates that metallic fuel operates at much lower temperatures than oxide fuel; therefore, the stored energy is correspondingly less.

Transient Results

The transient calculations simulated a station blackout with the reactor initially at full power (943 MWt IFR metal-core, 975 MWt CRBRP oxide-core). Electrical power to all the pumps was lost at 0.01 seconds and it was assumed the pony motors were unavailable. Reactor scram was delayed until 0.6 seconds. It was assumed the IFR metal-core decay power history was proportional to that of the CRBRP oxide-core. Because of transport delays, the behavior of the steam generating system during the first few minutes of the transient does not significantly affect the response of the primary system. Therefore, to reduce computing costs, the steam generating loop was decoupled from the calculations (an SSC-L option) following steady state initialization.

Previous calculations for the CRBRP have shown that natural circulation loop flows are adequate to remove core decay heat during a protected station blackout accident [5,6]. The present calculations demonstrate that the margin to boiling is greater for the IFR metallic core. Figure 5 compares the exit coolant temperature from the hot metallic fuel pin to the exit temperature from the hot oxide fuel pin. In both cases the coolant temperature remained well below saturation. For the metallic pin, the peak exit temperature was 97 K less than for the oxide pin[a] and, because of the faster thermal response time, occurred 22 seconds earlier. In each case the peak temperature was somewhat higher than its steady state value. Figure 6 compares average core outlet temperatures. The figure illustrates that the rate and also the magnitude of the change in coolant temperature is significantly greater for the metallic core (the same behavior was observed in Reference 7 for 1000 MWe LMFBR designs). Although the oxide fuel elements store more thermal energy, they give it up more slowly than metallic fuel elements. The metal-core outlet temperature may actually decrease at an unacceptable rate for CRBRP hot leg structures.

Figure 7 compares fuel centerline temperatures near the top of each fuel pin. The temperatures fell rapidly following reactor scram, but then increased until the decay heat generation rates decreased to the point where natural circulation provided adequate cooling. Again, these peaks were offset (by 10 seconds) and the maximum metal fuel temperature during the reheat period was 121 K less than the maximum oxide fuel temperature. In both cases, the maximum fuel temperature during the transition to natural circulation was less than during steady state operation. The power generated by each pin is also shown on Figure 7.

---

[a]The difference is partly due to the lower IFR core inlet temperature.

Additional Analyses

Some variations on the base case transient calculations were run to assess possible LMR design improvements. To scope the effect of a reduction in primary system pressure drop, as might be obtained by optimizing core lattice parameters or reducing orificing losses, the steady state pressure drop across the vessel (with IFR core) was decreased 20%. The results showed that the peak sodium outlet temperature decreased 16 K and that the natural circulation core flow rate at 200 seconds was 4.5% greater than before. The results for the oxide-core were similar.

Extending the primary pump coastdown has been suggested as one means of mitigating unprotected (i.e., failure to scram) loss-of-flow accidents. Loop-type LMR designs like the CRBRP employ a relatively rapid primary pump coastdown in order to minimize the thermal shock to hot leg structures. Nevertheless, the effect of an extended coastdown during a protected accident was evaluated by increasing the inertia of the primary coolant pumps such that the flow halving time increased from 6 to 22 seconds (5 to 19 seconds with the oxide core)[a]. The results showed a significant drop in the natural convective performance of the plant. Not only were fuel and coolant temperatures higher than before, but with the metallic core, coolant boiling was predicted in the average power fuel assemblies. This was the result of the partial collapse of the primary system temperature differential (lower hot leg temperatures and higher cold leg temperatures)[b]. As a consequence, the thermal driving head was insufficient to prevent near flow stagnation in the driver region (the flow was predicted to reverse in the radial blanket). Figure 8 compares coolant temperatures near the top of the average metallic and oxide fuel pins. As shown, coolant saturation was reached at 326 seconds with the metallic core. However, the oxide core, because of its slower thermal response time, did not boil. Adequate natural circulation was established by 340 seconds to turn the temperature transient around.

Two additional calculations were made where the flow halving time of the intermediate coolant pumps was also increased (from about 7 to 24 seconds metal-core, 7 to 23 seconds oxide-core). This time, the thermal driving head was adequate for a smooth transition from forced to natural circulation. The maximum metal-core coolant temperature was 58 K lower and occurred 198 seconds later than its base case. The maximum oxide-core coolant temperature was 54 K lower and occurred 194 seconds later than its base case. Figure 9 illustrates these results.

Figure 10 compares the metal-core extended coastdown core flow rates, and Figure 11 the metal-core extended coastdown upper and lower plenum coolant temperatures, with the base case results. For the extended coastdown cases, Figure 11 shows that the upper plenum coolant temperature decreased at an average rate of 3.6 K/s between 1 and 20 seconds compared to 1.9 K/s for the base case. Figure 11 also shows that thermal stratification occurred in the upper plenum of the reactor vessel for the

---

[a] The steam generating system was included in these calculations.

[b] It should be noted that this behavior is consistent with several tests conducted at EBR-II [8]. In the tests, the reactor was scrammed with the primary pumps left running. After the primary system had cooled down, power to the pumps was disconnected. The resulting peak coolant temperatures were higher than in tests with initially larger core inlet-to-outlet temperature differentials.

normal pump coastdown but not for the extended pump coastdowns. The results for the oxide-core were similar and are shown in Figures 12 and 13. For the oxide-core extended coastdown cases, the upper plenum coolant temperature decreased at an average rate of 2.5 K/s between 1 and 20 seconds compared to 0.8 K/s for the base case.

Two unprotected loss-of-flow accident calculations were also attempted. The base case station blackout and the extended pump coastdown calculation (both with IFR core) were run using the SSC-L point-kinetics model with preliminary IFR reactivity feedback data. Because SSC-L will currently only simulate prompt reactivity feedback effects (Doppler, coolant density, and fuel thermal expansion), both calculations predicted coolant boiling in the hot subchannel within one minute. However, the onset of boiling occurred 40 seconds later for the extended pump coastdown case. More realistic simulations of unprotected accidents will require that core radial expansion and control rod drive expansion reactivity feedback models be developed for SSC-L.

Summary

The analysis simulated a protected station blackout accident in a loop-type LMR containing a metallic core. The core design was based on ANL's Integral Fast Reactor (IFR) concept and the vessel and heat transport system were based on the CRBRP design. The results showed that fuel and coolant temperatures were lower than those predicted for the oxide-fueled CRBRP station blackout. However, the cooldown transient was more severe with the metallic core. A variation on the base case metal-core calculation showed that a 20% reduction in vessel pressure drop (under normal operating conditions) would increase the primary loop natural circulation flow rate by 4.5%. Extending the primary pump coastdown (flow halving time increased from 6 to 22 seconds metal-core, 5 to 19 seconds oxide-core) resulted in much higher fuel and coolant temperatures than the normal coastdown cases. The partial collapse of the primary system temperature differential resulted in near flow stagnation and coolant boiling in part of the metallic core before adequate natural circulation could be established. However, the oxide core, because of its slower thermal response time, did not boil. Increasing the flow coastdown times of both the primary and the intermediate coolant pumps allowed a smooth transition to natural circulation and reduced the maximum base case coolant temperatures by more than 50 K.

Acknowledgment

This work was supported by the U.S. Department of Energy under DOE Contract No. DE-AC07-76ID01570.

References

1. J. G. Guppy et al., Super System Code (SSC, Rev. 0), An Advanced Thermohydraulic Simulation Code for Transients in LMFBRs, NUREG/CR-3169, BNL-NUREG-51650, April 1983.

2. Y. I. Chang, J. F. Marchaterre, and R. H. Sevy, The Integral Fast Reactor Concept, Trans. Am. Nucl. Soc., 47, pp. 293-294, 1984.

3. Y. Orechwa and H. Khalil, Performance Characteristics of a Preliminary 330 MWe Metal Core Design, ANL-IFR-4, November 1984.

4. J. H. Kittel et al., Properties of Fuels for Alternate Breeder Fuel Cycles, ANL-AFP-38, May 1977.

5. G. J. Van Tuyle, Analysis of CRBRP Station Blackout Using SSC/MINET, BNL-NUREG-31110, 1982.

6. J. G. Guppy, W. C. Horak, and G. J. Van Tuyle, Independent Assessment of the Natural-Circulation Capability of the Heterogeneous Core CRBR, Trans. Am. Nucl. Soc., 45, pp. 416-417, 1983.

7. D. Saphier and J. T. Madell, A Comparative Transient Analysis of Metal and Oxide Fueled LMFBR, ANL-CT-80-1, September 1979.

8. R. M. Singer et al., "Studies Related to Emergency Decay Heat Removal in EBR-II," Proceedings of the International Meeting on Fast Reactor Safety Technology, Seattle, WA, August 19-23, 1979, Volume III, pp. 1590-1598.

Table 1. Comparison of IFR and CRBRP Core Design Parameters

	IFR	CRBRP
Core Configuration	Homogeneous	Heterogeneous
Thermal Power (MW)	943	975
Power Distribution		
Driver (%)	94.3	72.1
Internal Blanket (%)	-	17.1
Radial Blanket (%)	5.2	10.3
Control, Shield, Bypass (%)	0.5	0.5
Total Flow Rate (kg/s)	4558	5228
Flow Distribution		
Driver (%)	89.8	67.4
Internal Blanket (%)	-	15.4
Radial Blanket (%)	9.0	11.8
Control, Shield, Bypass (%)	1.2	5.3
Vessel Inlet Temperature (K)	630	671
Vessel Outlet Temperature (K)	793	818
Vessel Pressure Drop (kPa)	(662)	871
No. Driver Assemblies	108	162
No. Blanket Assemblies		
Internal	-	76
Radial	42	126
No. Control Assemblies	13	15
Pins per Driver Assembly	271	217
Pins per Blanket Assembly	127	61
Pins per Control Assembly	(37)	37
Driver Pin Design		
Pin Diameter (mm)	7.112	5.842
Fuel Diameter (mm)	5.367	4.915
Clad Thickness (mm)	0.457	0.381
Pitch/Diameter	1.21	1.25
Fuel Length (mm)	914.4	914.4
Lower Axial Blanket Length (mm)	355.6	355.6
Upper Axial Blanket Length (mm)	355.6	355.6
Gas Plenum Length (mm)	914.4	1219.2
Fuel Material	U-Pu-Zr	UO_2-PuO_2
Axial Blanket Material	U	UO_2
Blanket Pin Design		
Pin Diameter (mm)	11.633	12.852
Blanket Diameter (mm)	9.882	11.938
Clad Thickness (mm)	0.457	0.381
Pitch/Diameter	1.08	1.07
Blanket Length (mm)	1625.6	1625.6
Gas Plenum Length (mm)	914.4	1159.0
Blanket Material	U	UO_2

Table 2. Comparison of IFR and CRBRP Initial Operating Conditions

	IFR	CRBRP
Power Generation (kW)		
Hot Pin	40.9	26.0
Average Pin	30.4	20.0
Maximum Linear Power (kW/ft)		
Hot Pin	15.9	10.1
Average Pin	11.8	7.8
Maximum Fuel Temperature (K)		
Hot Pin	1001	2163
Average Pin	922	1826

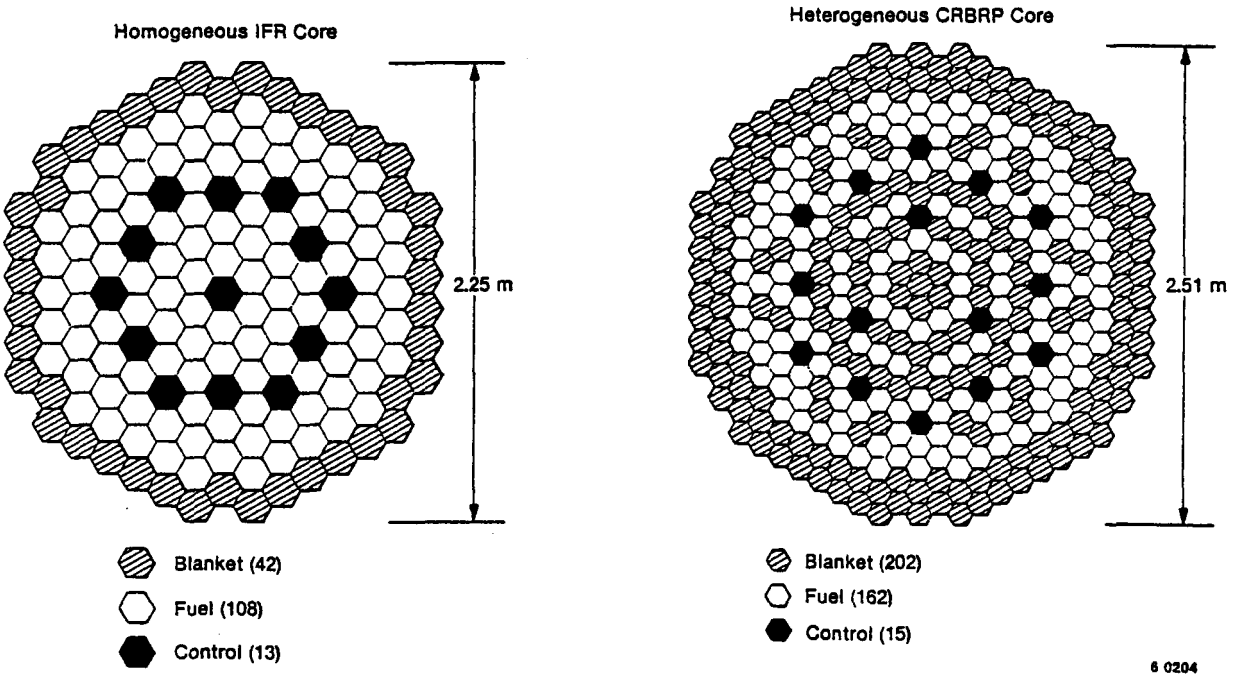

Figure 1. Comparison of IFR and CRBRP core configurations.

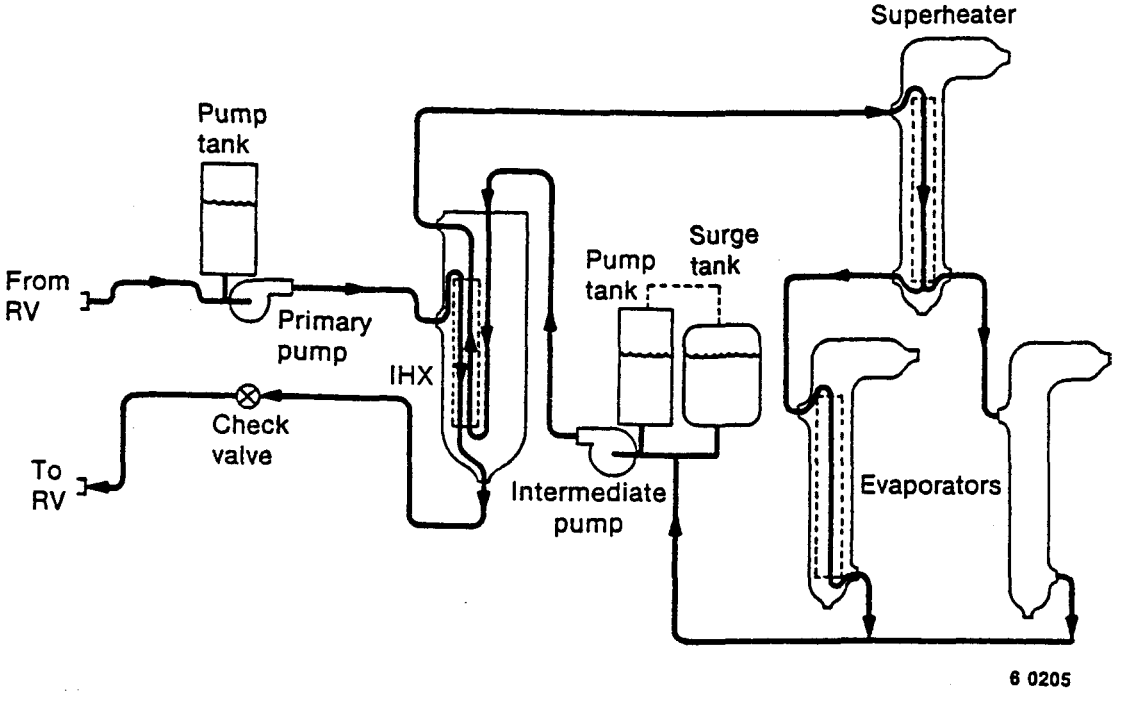

Figure 2. CRBRP heat transport system configuration.

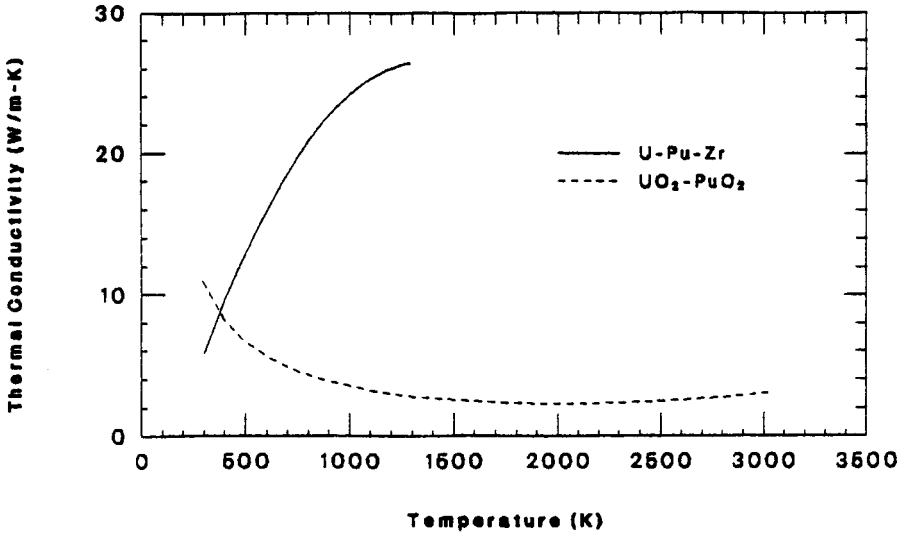

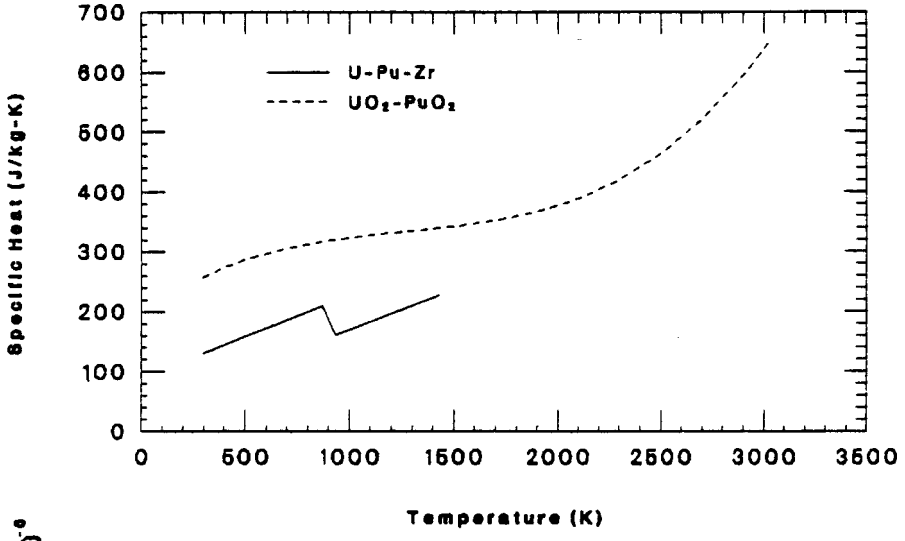

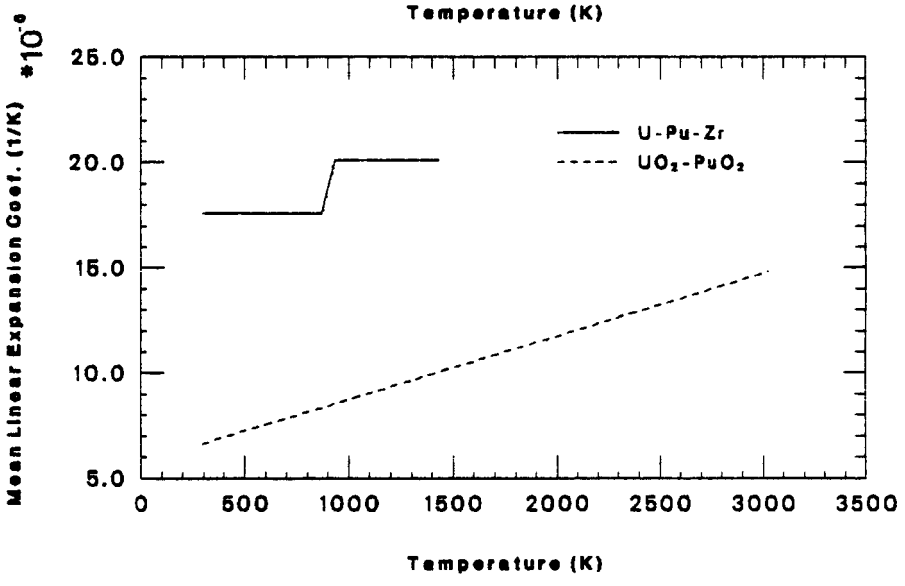

Fig. 3 Comparison of metal and oxide fuel thermal properties (metal fuel thermal conductivity extrapolated above 1073 K).

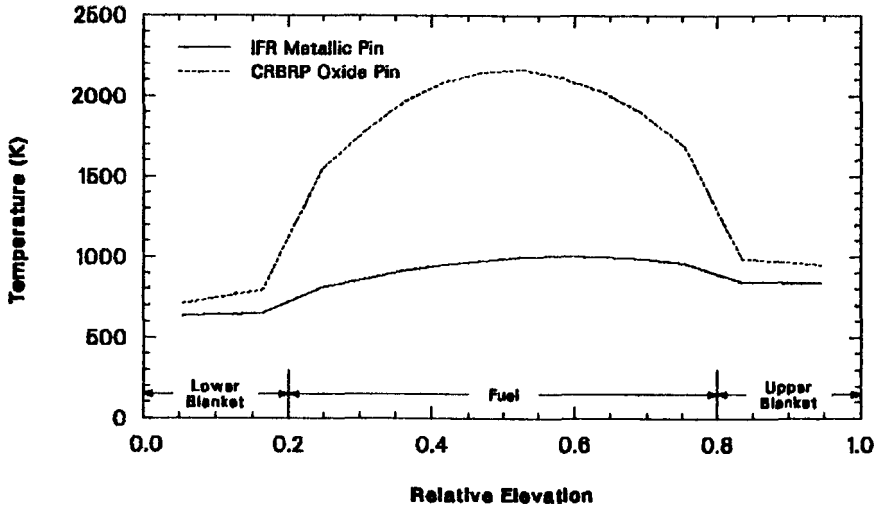

Fig. 4 Comparison of IFR and CRBRP hot pin centerline temperature profiles during steady state operation.

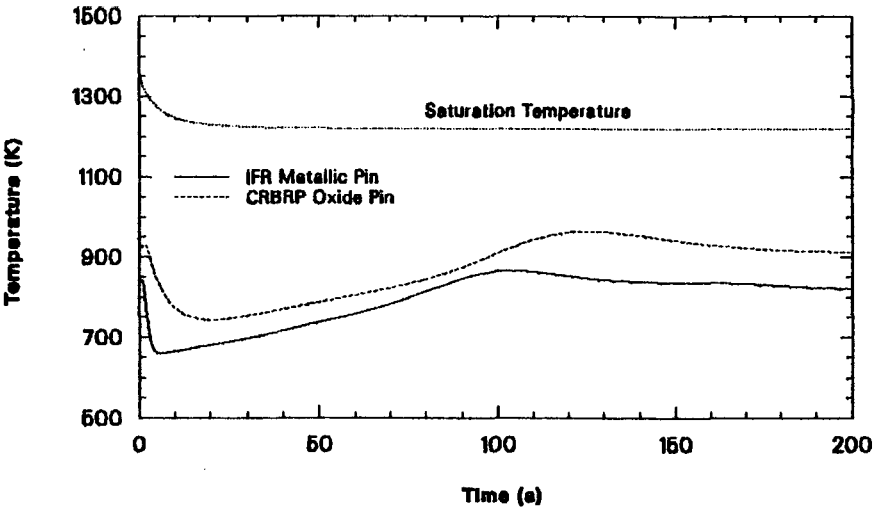

Fig. 5 Comparison of IFR and CRBRP hot channel outlet temperatures during protected station blackout .

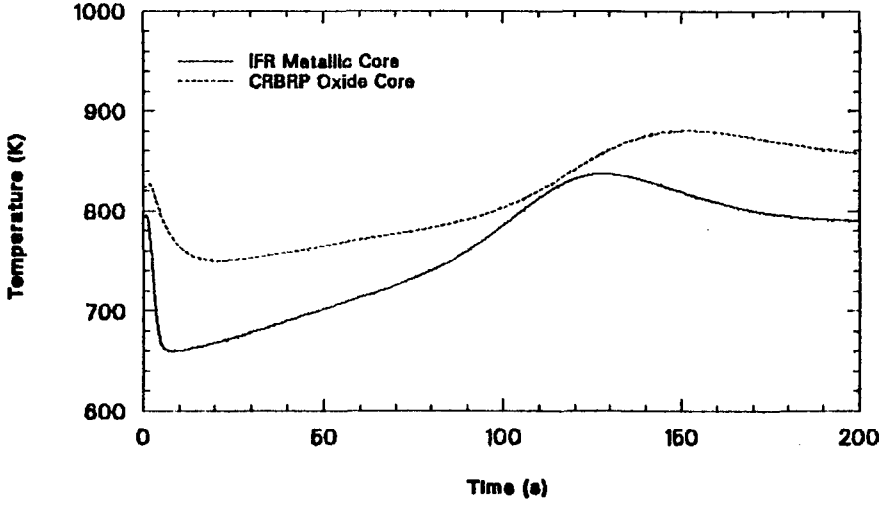

Fig. 6 Comparison of IFR and CRBRP average core outlet temperatures during protected station blackout .

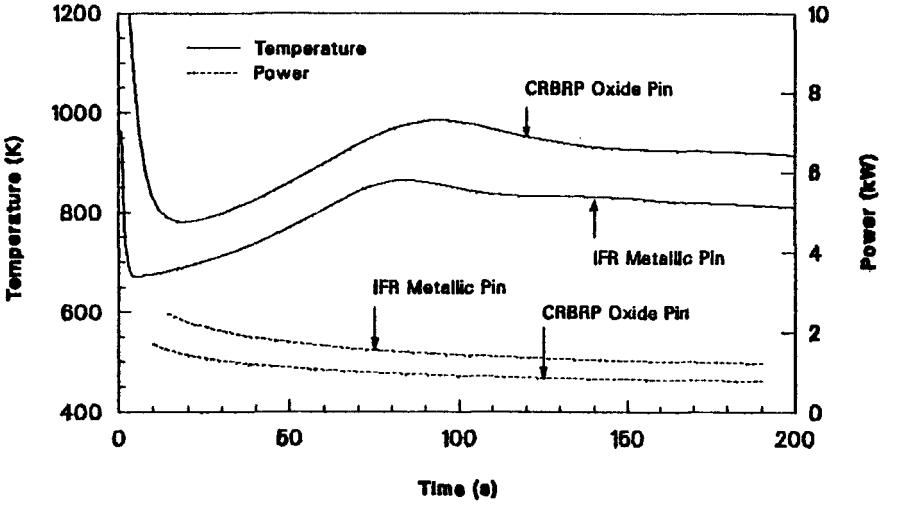

Fig. 7 Comparison of IFR and CRBRP hot pin centerline temperatures and power histories during protected station blackout .

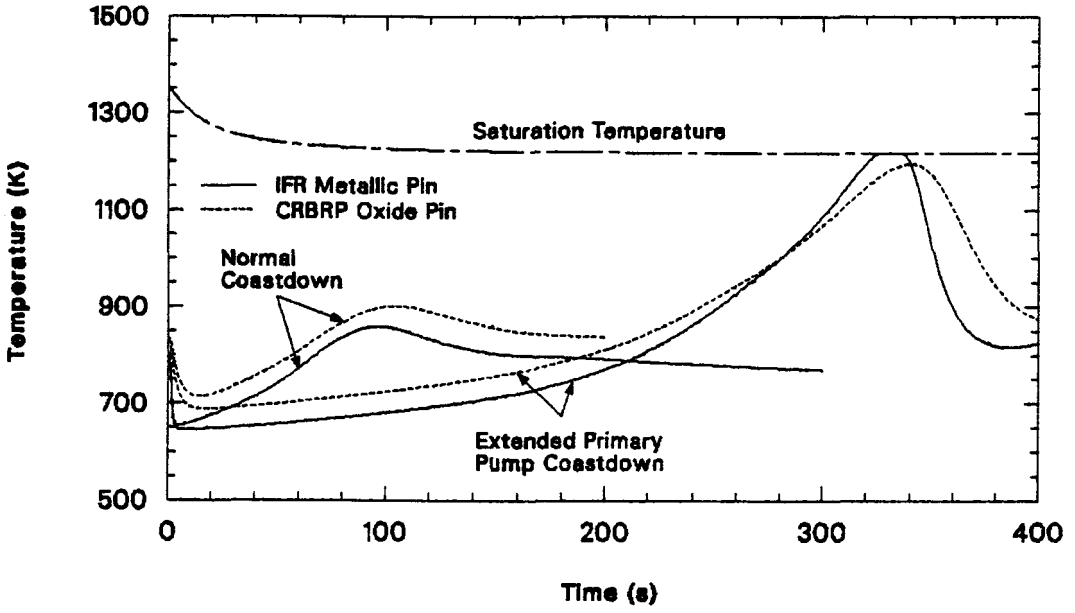

Fig. 8 Comparison of IFR and CRBRP peak coolant temperatures during protected station blackout (extended primary pump coastdown).

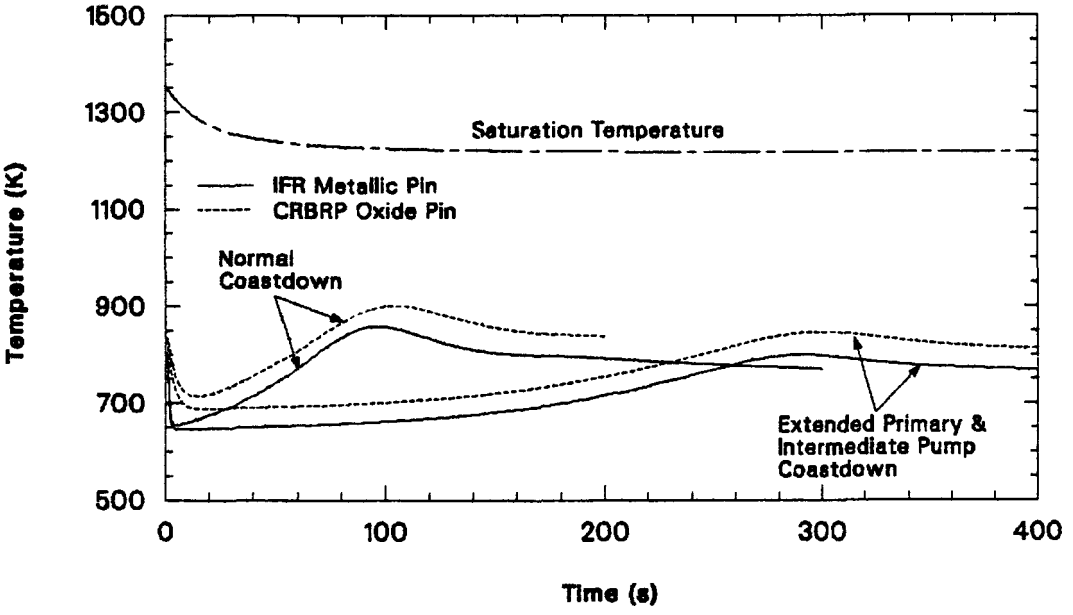

Fig. 9 Comparison of IFR and CRBRP peak coolant temperatures during protected station blackout (extended primary and intermediate pump coastdown).

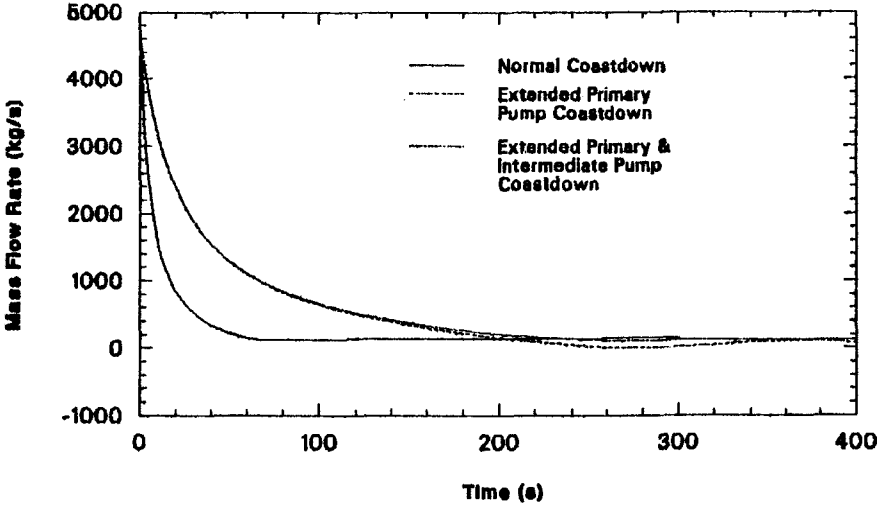

Fig. 10 Comparison of normal- and extended-coastdown core flow rates during protected station blackout (metal-core) .

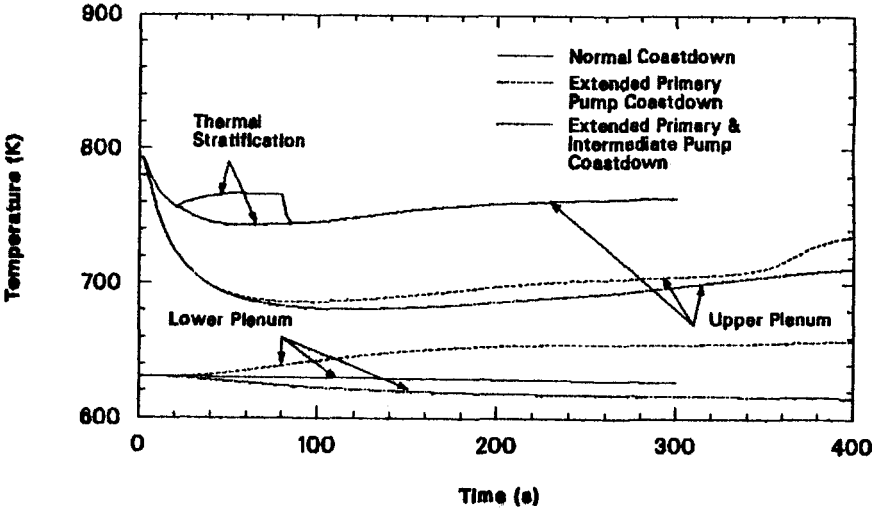

Fig. 11 Comparison of normal- and extended-coastdown upper and lower plenum coolant temperatures during protected station blackout (metal-core) .

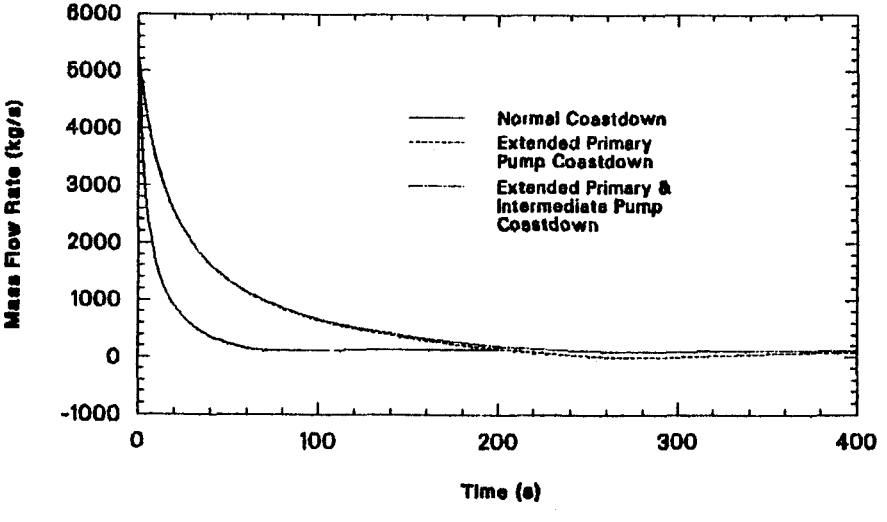

Fig. 12 Comparison of normal- and extended-coastdown flow rates during protected station blackout (oxide-core) .

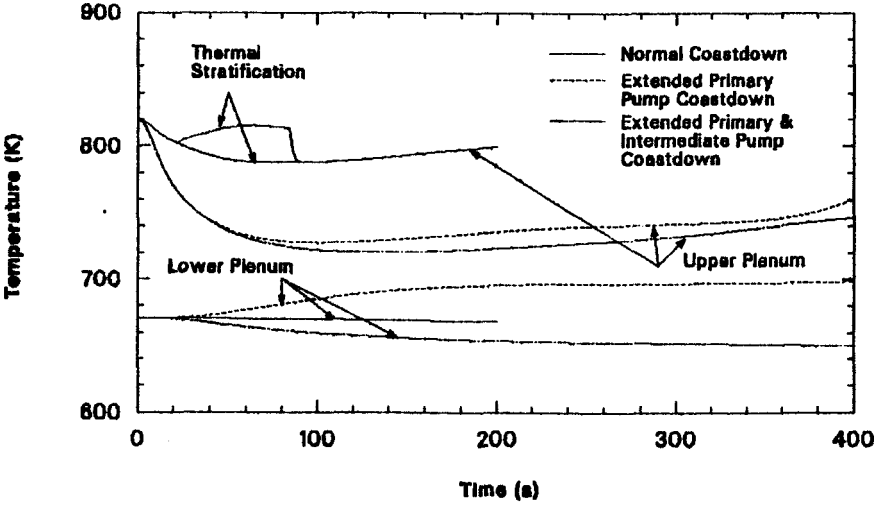

Fig. 13 Comparison of normal- and extended-coastdown upper and lower plenum coolant temperatures during protected station blackout (oxide-core) .